ResearchGate

See discussions, stats, and author profiles for this publication at: https://www.researchgate.net/publication/249965532

New Interfacial Microtubule Inhibitors of Marine Origin, PM050489/PM060184, with Potent Antitumor Activity and a Distinct Mechanism

ARTICLE *in* ACS CHEMICAL BIOLOGY · JULY 2013

Impact Factor: 5.33 · DOI: 10.1021/cb400461j · Source: PubMed

CITATIONS
9

READS
61

14 AUTHORS, INCLUDING:

Isabel Barasoain
Spanish National Research Council
103 PUBLICATIONS **1,646** CITATIONS
SEE PROFILE

Ruth Matesanz
Spanish National Research Council
21 PUBLICATIONS **434** CITATIONS
SEE PROFILE

Jesús Jiménez-Barbero
Center for Cooperative Research in Biosciences
541 PUBLICATIONS **10,321** CITATIONS
SEE PROFILE

Jose Manuel Andreu
Centro de Investigaciones Biológicas
166 PUBLICATIONS **5,765** CITATIONS
SEE PROFILE

Available from: Javier Rodríguez-Salarichs
Retrieved on: 31 January 2016

ACS chemical biology

Articles

pubs.acs.org/acschemicalbiology

New Interfacial Microtubule Inhibitors of Marine Origin, PM050489/PM060184, with Potent Antitumor Activity and a Distinct Mechanism

Benet Pera,[†,§] Isabel Barasoain,[†] Areti Pantazopoulou,[†] Angeles Canales,[†] Ruth Matesanz,[†] Javier Rodriguez-Salarichs,[†] Luis F. García-Fernandez,[‡] Victoria Moneo,[‡] Jesús Jiménez-Barbero,[†] Carlos M. Galmarini,[‡] Carmen Cuevas,[‡] Miguel A. Peñalva,[†] J. Fernando Díaz,*[,†] and José M. Andreu*[,†]

[†]Centro de Investigaciones Biológicas, CSIC, Ramiro de Maeztu 9, 28040 Madrid, Spain

[‡]PharmaMar S.A., Avda de los Reyes 1, Polígono Industrial La Mina, Colmenar Viejo, 28770 Madrid, Spain

Supporting Information

ABSTRACT: We have investigated the target and mechanism of action of a new family of cytotoxic small molecules of marine origin. PM050489 and its dechlorinated analogue PM060184 inhibit the growth of relevant cancer cell lines at subnanomolar concentrations. We found that they are highly potent microtubule inhibitors that impair mitosis with a distinct molecular mechanism. They bind with nanomolar affinity to unassembled $\alpha\beta$-tubulin dimers, and PM050489 binding is inhibited by known Vinca domain ligands. NMR TR-NOESY data indicated that a hydroxyl-containing analogue, PM060327, binds in an extended conformation, and STD results define its binding epitopes. Distinctly from vinblastine, these ligands only weakly induce tubulin self-association, in a manner more reminiscent of isohomohalichondrin B than of eribulin. PM050489, possibly acting like a hinge at the association interface between tubulin heterodimers, reshapes Mg^{2+}-induced 42 S tubulin double rings into smaller 19 S single rings made of 7 ± 1 $\alpha\beta$-tubulin dimers. PM060184-resistant mutants of *Aspergillus nidulans* map to β-tubulin Asn100, suggesting a new binding site different from that of vinblastine at the associating β-tubulin end. Inhibition of assembly dynamics by a few ligand molecules at the microtubule plus end would explain the antitumor activity of these compounds, of which PM060184 is undergoing clinical trials.

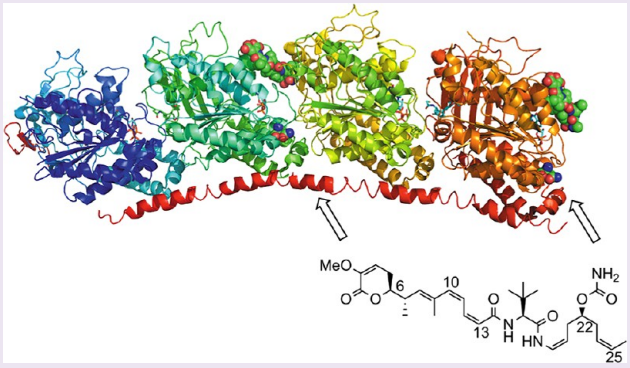

Tubulin is a major cytoskeletal protein in most eukaryotic cells, where it assembles to form microtubules. Among the multiple cellular processes in which microtubules are involved, intracellular transport, the proper attachment of chromosomes to the spindle, and the complex movements of the chromosomes during mitosis, including their alignment and separation,[1] are essential for cell division and survival. These essential functions make tubulin an evident target for anticancer drugs.[2] Tubulin-binding agents (TBA), either microtubule inhibitors that bind to unassembled tubulin or stabilizing agents that bind to microtubules, modify the growing and shrinking dynamics of these polymers, which is essential for correct chromosome segregation. The dividing tumor cells treated with these compounds become blocked or undergo aberrant mitosis, resulting in cell death.[1] Among TBA, vinblastine derivatives,[3] paclitaxel,[4] and docetaxel[5] are widely used for the treatment of several types of cancer.[6] Microtubules remain a valid target for cancer chemotherapy. Recently, cabazitaxel (a paclitaxel derivative)[7] and ixabepilone (an epothilone B analogue)[8] were introduced. Eribulin, a synthetic truncated form of homohalichondrin, has more recently been approved for the treatment of metastatic breast cancer.[9]

However, despite the clinical interest of TBA and new antitumor agents, which combined with other treatments have significantly increased the rate of success of the anticancer therapy, there is still an urgent need to search for new compounds with which to address the known problem of drug resistance.[10] Although chemotherapeutic treatment of cancers is important to combat these diseases, it often fails due to the development of the tumor multidrug resistance (MDR) phenotype,[11] so it could be considered that all cancer-related deaths are a result of chemotherapeutic failure.[12]

Marine multicellular life appeared 1 billion years ago, whereas the oldest generally accepted remains of land plants date back to the Ordovician period about 500 million years ago. Thus, the large biological diversity of marine compounds and their high potency, related to the dilution effect in a sea environment,[13] indicates that among all sources of TBA, marine organisms are a very promising source of new antitumor drugs.[14,15]

Received: May 6, 2013
Accepted: July 16, 2013
Published: July 16, 2013

ACS Publications © 2013 American Chemical Society

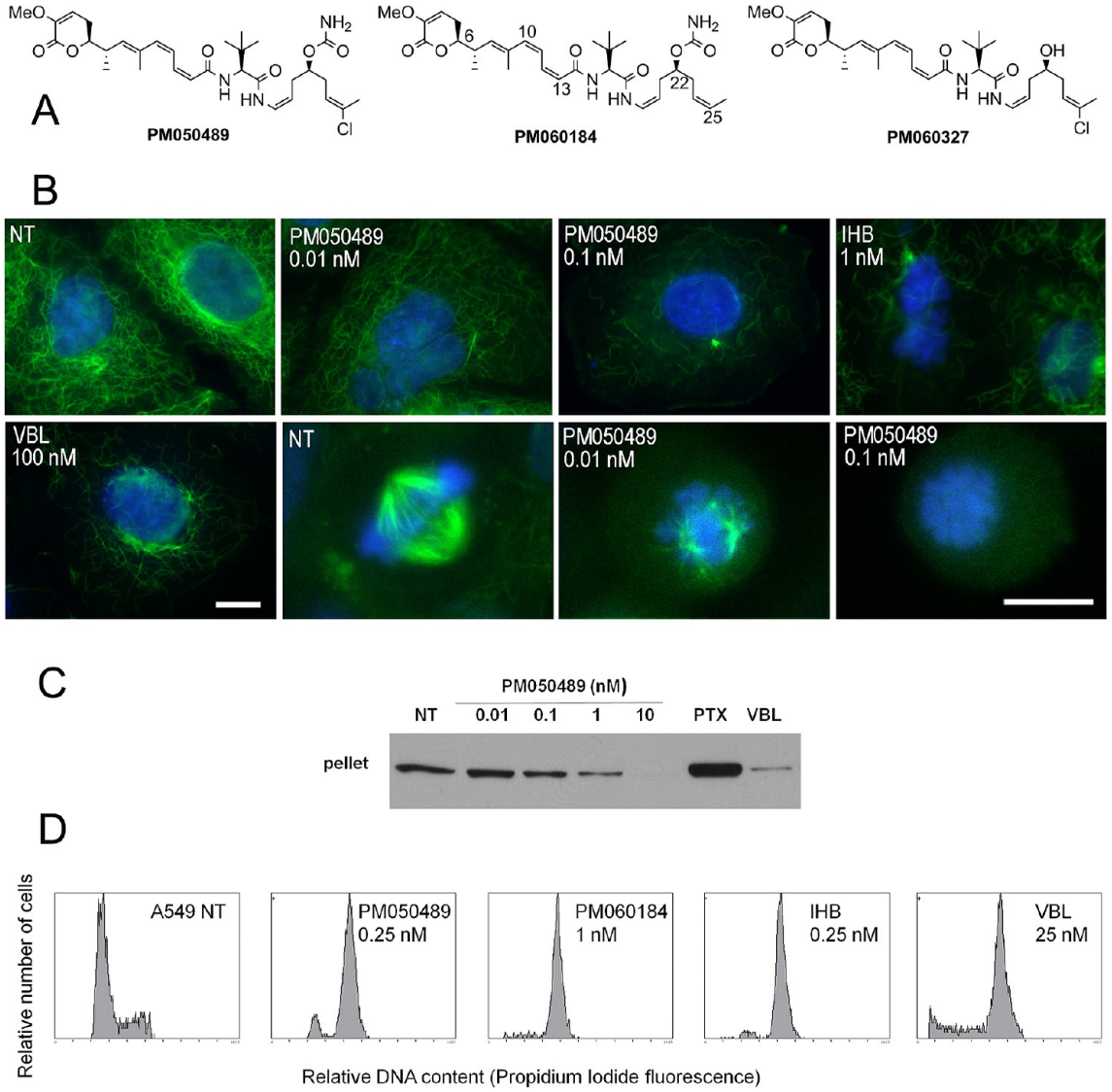

Figure 1. PM050489 is a potent microtubule depolymerizing agent. (A) Chemical structures of PM050489 and the analogues employed. (B) Effects of PM050489 as compared to isohomohalichondrin B (IHB) and vinblastine (VBL) on the microtubule network in interphase cells and on mitotic spindle morphology. A549 cells were incubated for 24 h with 0.5% dimethylsulfoxide vehicle (nontreated, NT), 0.01 or 0.1 nM PM050489, 1 nM IHB, or 100 nM VBL. The three last panels show mitotic cells. Microtubules were immunostained with α-tubulin monoclonal antibodies, and DNA was stained with Hoechst 33342. The scale bar represents 10 μm, as indicated in the VBL panel for the first five panels and in the last panel for the last three panels. (C) Effects of PM060489 on the polymerized tubulin pool of A549 cells, compared to paclitaxel (PTX, 100 nM) and VBL (100 nM). (D) Effects of PM050489 and PM060184 on the cell cycle of A549 cells compared to IHB and VBL. Cells were incubated for 20 h with either DMSO or drugs. The drug concentration depicted is the lowest concentration that causes ≥90% cell arrest in the G_2/M phase of the cell cycle.

PM050489 and its dechlorinated analogue PM060184 (Figure 1A) are a new class of compounds isolated from the marine sponge *Lithoplocamia lithistoides*; both are currently obtained by total synthesis,[16] and PM060184 is undergoing phase I clinical trials in the oncology setting. We have identified their target and mechanism of action, employing cell biology, biochemical, and biophysical approaches. Our results show that these compounds potently disrupt cellular microtubules and mitosis and thus inhibit the proliferation of tumor cell lines. They bind with uniquely high affinity to $\alpha\beta$-tubulin dimers, inhibiting vinblastine binding at the association interface between them, but distinctly modulating tubulin association reactions, which gives insight into the inhibition of microtubule assembly by these small molecules.

RESULTS AND DISCUSSION

New Microtubule Inhibitors with Potent Antiproliferative Activity. The cell growth inhibitory activities of PM050489 and PM060184 were determined using a panel of 23 tumor cell lines representing 10 relevant types of human cancer, all of which were very sensitive to the treatment. The GI_{50} values ranged from 20 pM to 5 nM and were considerably lower than those of the widely used antitumor drugs vinblastine (VBL) and paclitaxel (Supplementary Table S1).

We found that these two compounds very powerfully disrupt cellular microtubules (Figure 1B and C). Control A549 lung carcinoma cells presented organized cytoplasmic microtubule networks and normal metaphase mitotic spindles, with condensed chromosomes in a compact metaphase plate located midway between the two spindle poles. Cells treated with such

dx.doi.org/10.1021/cb400461j | *ACS Chem. Biol.* 2013, 8, 2084−2094

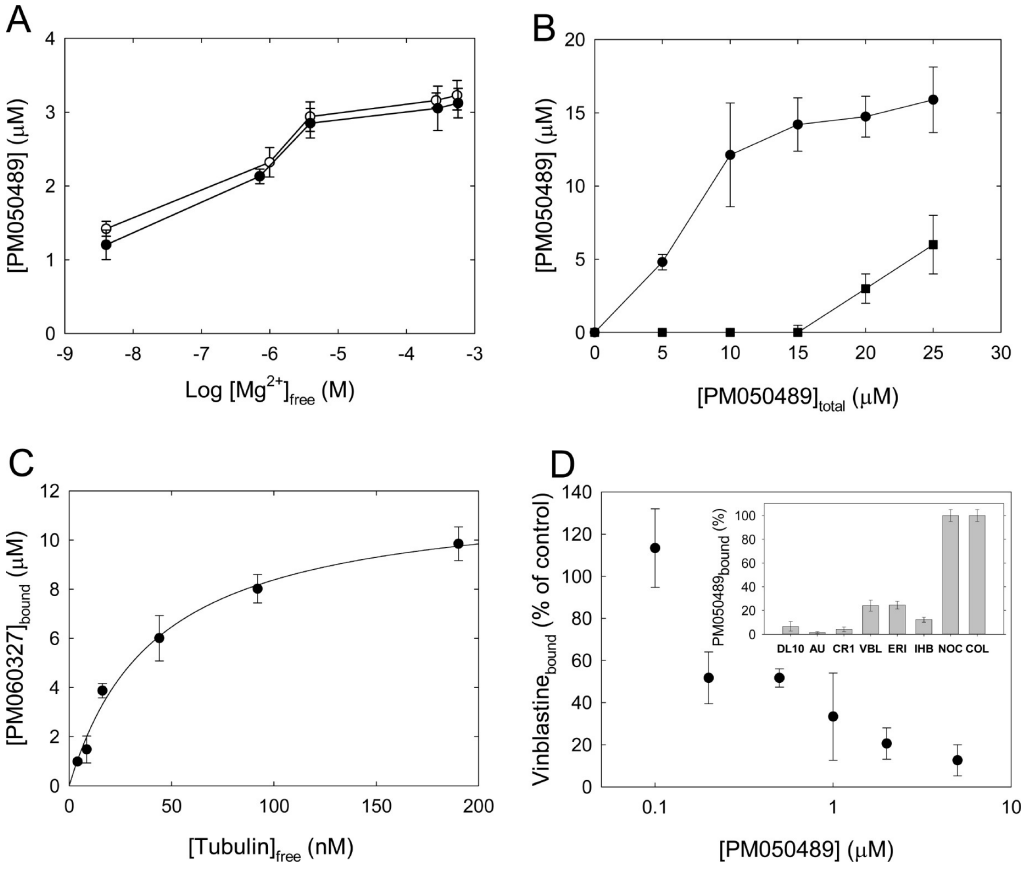

Figure 2. Biochemical characterization of the tubulin-PM050489 interaction. (A) Dependence of PM050489 binding to unassembled tubulin on the free Mg^{2+} concentration. Four micromolar GDP-tubulin (filled circles) or GTP-tubulin (empty circles) was incubated with 5 μM total PM050489 at different $MgCl_2$ concentrations in PE buffer/0.1 mM GXP at 37 °C. (B) Stoichiometry of PM050489 binding to unassembled tubulin (15 μM) in with 0.27 mM free Mg^{2+} (1.5 mM $MgCl_2$). (Solid circles and squares are bound and free PM050489, respectively). (C) Isotherm of binding of PM060327 by dimeric tubulin under the same conditions. (D) Inhibition of 0.5 μM H^3-vinblastine binding to 0.5 μM dimeric tubulin by PM050489. Inset: inhibition of 4 μM PM050489 binding to 6 μM tubulin by 50 μM dolastatin 10 (DL10), auristatin (AU), cryptophicin 1 (CR1), vinblastin (VBL), eribulin (ERI), isohomohalichondrin (IBH), nocodazol (NOC), and colchicine (COL); bars represent standard errors of three independent experiments.

a low concentration as 10 pM PM050489 had fewer, disorganized, cytoplasmic microtubules. Mitotic cells showed aberrant (bipolar, monopolar, and multipolar) metaphase spindles with an accumulation of condensed chromatin (corresponding to the described type I, II, and III spindles[17]). Treatment with 100 pM PM050489 markedly disrupted the interphase and the mitotic spindle microtubules (with condensed chromosomes remaining, corresponding to type IV spindles[17]). Similar results were obtained with PM060184 at concentrations slightly higher than those of PM050489. Higher concentrations of isohomohalichondrin B (IHB) (×10) or VBL (×10^3) were required to inhibit A549 microtubules (Figure 1B). PM050489 did not affect the actin cytoskeleton of PtK2 cells (Supplementary Figure S1).

Consistent with their microtubule inhibitory activity, these compounds induced A549 cell cycle arrest in the G_2/M phase, which was maximal at 0.25 nM PM050489, 1 nM PM060184, 0.25 nM IHB, or 25 nM VBL (Figure 1D) (similar effects were produced by 0.2 nM dolastatin, 0.2 nM cryptophicin, or 5 nM eribulin).

We observed that the *in vitro* assembly of tubulin into microtubules was efficiently inhibited by PM050489 and PM060184. The critical concentration of tubulin required for assembly in our assay increased from 3.30 ± 0.02 μM (without compound) to 9.9 ± 1.3 μM and 13.8 ± 1.5 μM in the presence of a 10% molar excess of PM050489 or PM060184, respectively (Supplementary Figure S2A). The remaining microtubules showed a normal morphology, and no aberrant polymers were found.

These results indicated that PM050489 and PM060184 powerfully inhibit cellular microtubules, possibly by targeting tubulin self-assembly, and thus impair mitosis and cell growth. Their antiproliferative potency compares very favorably with those reported for the most active microtubule inhibitors of marine origin: dolastatin 10, cryptophicin 1,[18] halichondrin B, or the antitumor drug eribulin.[19]

PM050489, PM060184, and PM060327 Bind with Nanomolar Affinity to $\alpha\beta$-Tubulin Dimers and Inhibit the Binding of Vinca Domain Ligands. We sought to measure the interaction of these inhibitors with tubulin and to map their binding site. We observed that each of these ligands (4 μM) completely co-sedimented with an excess of unassembled tubulin (5 μM) upon high-speed centrifugation and HPLC analysis, indicating binding with submicromolar affinity (Supplementary Figure S2B). However, binding of PM050489 to microtubules was not detectable (which does not exclude binding to a small fraction of the assembled tubulin molecules). These features suggested that PM050489 was

dx.doi.org/10.1021/cb400461j | ACS Chem. Biol. 2013, 8, 2084−2094

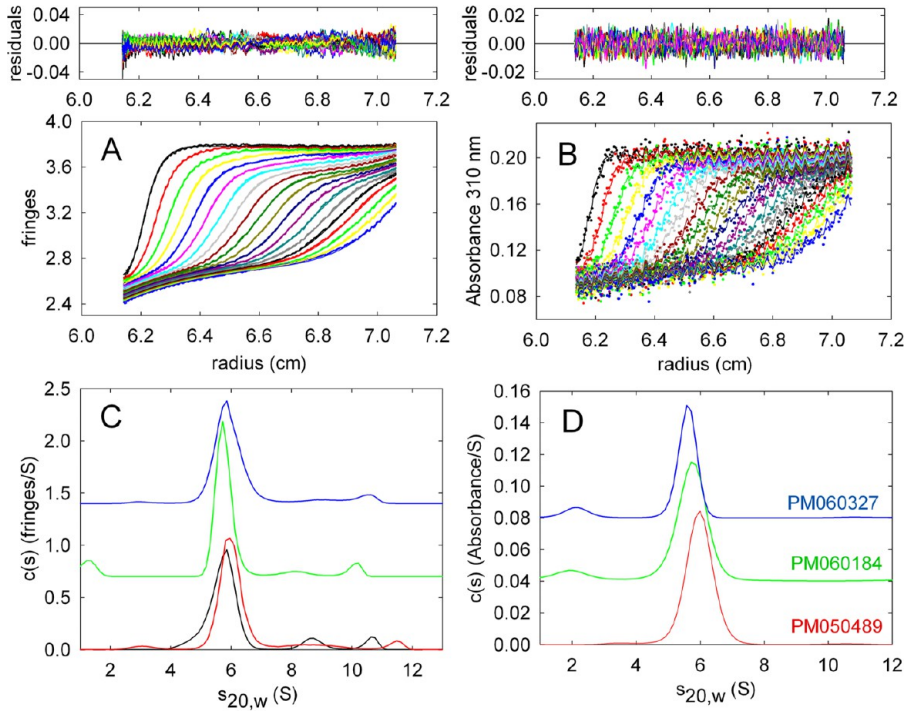

Figure 3. Binding to tubulin of PM050489 and its analogues analyzed by sedimentation velocity. (A) Successive radial interference scans showing the distribution of tubulin (4 μM) in the presence of PM050489 (5 μM) during sedimentation in the analytical ultracentrifuge, in PE buffer/1.5 mM $MgCl_2$/0.1 mM GTP at 25 °C. Only one from each two scans is shown. (B) Corresponding radial scans showing the co-sedimentation of PM050489 in the same experiment, obtained by measuring the absorbance at 310 nm. (C) Sedimentation coefficient distribution $c(s)$ of 4 μM tubulin without ligand (black line, main peak average $s_{20,w}$ = 5.6 S), with 5 μM PM050489 (red, 6.0 S), PM060184 (green, 5.8 S), and PM060327 (blue, 5.7 S). (D) Corresponding sedimentation coefficient distributions of each ligand (same color code as panel C; 6.0, 5.7, and 5.6 S respectively). From the area under the main peaks and the initial concentrations it was calculated that 1.3 PM050489, 1.2 PM060184 or 1.1 PM060327 molecules co-sedimented per tubulin dimer.

disrupting some of the tubulin polymerization interfaces. Binding of PM050489 to GTP-tubulin or GDP-tubulin requires Mg^{2+} ions, increasing from weak at ~10 nM free Mg^{2+} to maximal around 10 μM free Mg^{2+} (Figure 2A). This could be an effect of the binding of one high affinity Mg^{2+} ion to tubulin.[20]

Co-sedimentation experiments indicated that each $\alpha\beta$-dimer of tubulin binds one molecule of PM050489, in PE buffer with 0.27 mM free Mg^{2+} (10 mM sodium phosphate, 1 mM EDTA, 0.1 mM GTP, pH 7.0 with 1.5 mM $MgCl_2$) (Figure 2B). In order to facilitate biochemical and NMR studies of interaction with tubulin, the slightly more soluble analogue PM060327 with a hydroxyl instead of a carbamate group at position 22 was employed (Figure 1A). Titration of PM060327 (10 nM) with tubulin (5−200 nM) in co-sedimentation experiments (Figure 2C) indicated K_d = 41 ± 9 nM. The higher binding affinities of PM050489 and PM060184 could hardly be measured directly, but competition experiments with PM060327 afforded 10-fold and 4-fold smaller K_d values, 4.1 ± 1.0 nM and 10 ± 2 nM, respectively.

We found that PM050489 and the two analogues inhibit the binding of VBL to tubulin (Figure 2D) and that VBL and the "Vinca domain" ligands dolastatin 10, auristatin, cryptophicin 1, eribulin (ERI), and isohomohalichondrin B (IHB), but not nocodazole or colchicine, inhibited PM050489 binding (Figure 2D inset). PM050489 did not inhibit the binding of the fluorescent ligand MTC to the colchicine site,[21] which is located at the intradimer association interface.[22] These inhibitory features of PM050489 binding suggested its interaction with the tubulin intradimer interface similarly to VBL, which binds between two tubulin dimers in the complex with the RB3 protein stathmin-like domain (SLD)[23] and is considered a paradigm interfacial inhibitor.[24]

We then asked which tubulin association state primarily binds the new inhibitors. The functional assembly unit of tubulin is the tight $\alpha\beta$-heterodimer [$s^0_{20,w}$ = 5.8 $S^{20,25}$]. Simultaneous protein and ligand sedimentation velocity measurements by analytical ultracentrifugation (AUC) showed that PM050489, PM060184, and PM060327 co-sediment with S $\alpha\beta$-tubulin dimers (weight average $s^{0.5}_{20,w}$ = 5.8 ± 0.2) and supported 1:1 binding (Figure 3).

VBL also binds to tubulin in a unitary stoichiometry but with lower (micromolar) effective affinity values under closely related free Mg^{2+} and buffer conditions.[26] One key difference with PM050489 is that VBL binds to tubulin oligomers better than to $\alpha\beta$-dimers.[27] The very high binding affinities of PM050489 and its analogues for tubulin dimers surpass the affinities of the Vinca domain ligands dolastatin 10, cryptophycin 1,[18] halichondrin B, and eribulin.[28,29]

Molecular Recognition of PM060327 by Tubulin Dimers. In order to gain more detailed insight into the binding interactions, the conformation and the epitope of the inhibitor when bound to tubulin were analyzed using TR-NOESY and STD NMR methods.[30] Due to the low solubility of PM050489 and PM060184 the hydroxyl analogue PM060327 used to directly measure affinity (Figure 2C) was also employed for NMR experiments (Figure 4). Its cellular and *in vitro* microtubule inhibition effects were confirmed to be similar to those of PM050489 and PM060184. Negative NOESY crosspeaks were observed for PM060327 in the

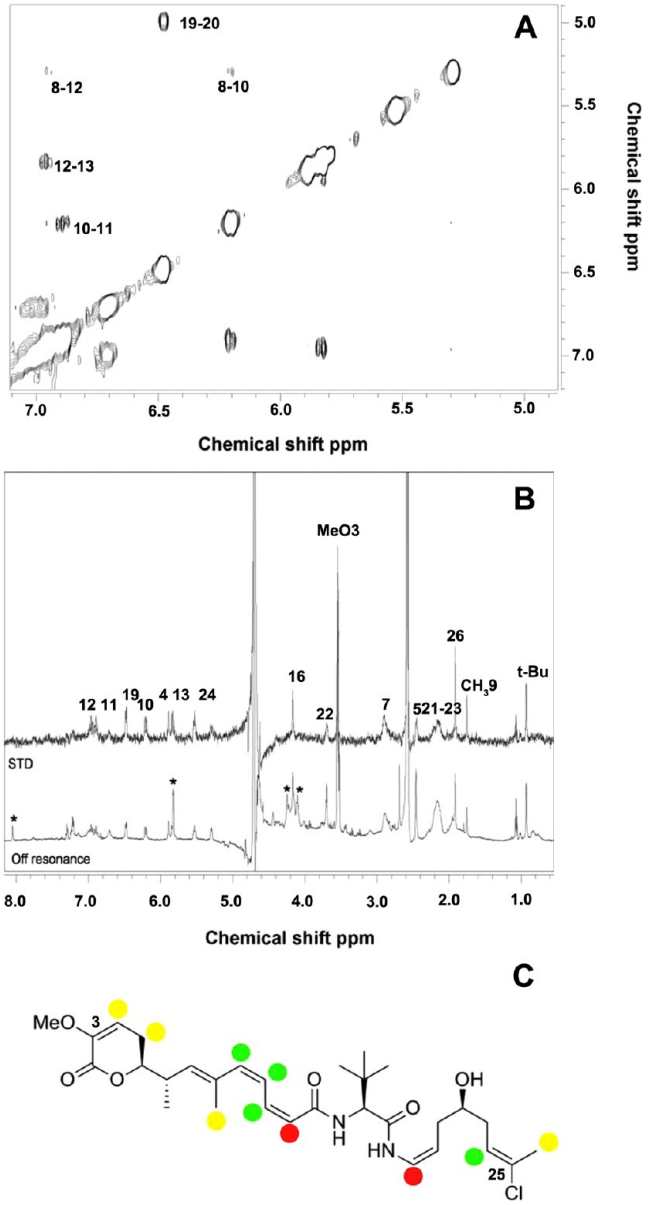

Figure 4. NMR characterization of the tubulin−PM060327 interaction. (A) TR-NOESY spectrum (mixing time 200 ms) of PM060327 (total 200 μM) in the presence of 5 μM tubulin dimers (in D_2O buffer with 7.5% d_6-DMSO). (B) Off-resonance (lower line) and STD spectra (upper line) of PM060327 (200 μM) with tubulin (5 μM). Peaks labeled with an asterisk come from GTP. (C) Epitope map of PM060327 binding to tubulin. Red circles indicate protons with an STD over 40%, green circles protons with an STD between 35% and 40%, and yellow circles protons with an STD between 25% and 35%.

presence of tubulin, indicating its effective binding (Figure 4A). Only cross peaks between vicinal protons were found, with no correlations between protons located far in the molecular sequence. This strongly suggests that the molecule adopts an extended bound conformation prior to dissociation. The solubility of PM060327 in the absence of tubulin was not enough to determine the conformation of the free ligand. The STD spectrum (Figure 4B) showed that hydrogens at the conjugated double bonds area (H10−H13) in the central part of the molecule, as well as those attached at positions C19, C24, and C26 at the Cl butenyl end, displayed the higher STD values, indicating their close contact with the protein binding site, followed by protons at positions C4 and C5 at the lactone ring end (Figure 4C). However, the STD of the *tert*-butyl group was comparatively weaker. Control sedimentation velocity measurements indicated that PM060327 binds to $\alpha\beta$-tubulin dimers and traces of oligomers (3%) under the NMR D_2O-dimethylsulfoxide (DMSO) buffer conditions (Supplementary Figure S3).

PM050489 Modulates Tubulin Self-Association Inducing Tubulin Single Ring Formation Similarly to Isohomohalichondrin B. Once it was established that PM050489 binds to tubulin dimers interfering with VBL binding, we compared the effects on tubulin self-association of this compound with a selection of ligands of the Vinca domain, employing AUC and electron microscopy (Figure 5). VBL binds like a wedge between the free plus end of the β-subunit from one heterodimer and the free minus end of the α-subunit from the next $\alpha\beta$-dimer.[23] VBL induces the association of tubulin dimers, even in the absence of Mg^{2+}, as well as Mg^{2+}-dependent tubulin spiral formation,[26,31] thus inhibiting proper assembly and suppressing microtubule dynamics.[6] The linkage of the VBL binding and tubulin self-association processes increases the observed VBL affinity.[26] On the other hand, halichondrins and the truncated analogue eribulin are noncompetitive inhibitors of VBL binding that do not induce spiral formation,[29,32,33] suggesting that they bind to tubulin dimers. We found that under conditions of incipient Mg^{2+}-induced tubulin self-association (5 μM tubulin with 1.13 mM free Mg^{2+}, in order to give maximal PM050489 binding), PM050489 induced only a weak association from 5.8 S tubulin dimers, increasing the tubulin weight average sedimentation coefficient to $s^{0.5}_{20,w}$ = 7.2 S (Figure 5A). IHB had a similar effect, whereas ERI lacked effect, and VBL induced a much stronger association with a main peak at 14 S. Interestingly, adding PM050489, IHB, or ERI practically reverted the action of VBL (Figure 5A), either by replacing it or by acting through the protein association (Figure 2D). PM050489, PM060184, and PM060327 had similar effects (Supplementary Figure S4).

We next examined the effects of PM050489 on Mg^{2+}-induced tubulin double ring formation. Tubulin rings are the curved end-product of inactive tubulin self-association, which are also observed upon disassembly of initially straight microtubule protofilaments.[25,34−37] Spiral tubes can form when ring closure does not take place.[38] We found that under conditions of oligomerization and incipient double-ring formation (100 μM GTP-tubulin at 6.7 mM free Mg^{2+}), PM050489 induced a major 14.8 S peak (Figure 5B). Apparently single-wall rings of 25.4 ± 0.9 nm (n = 33) outer diameter were observed by electron microscopy, in contrast to a few double rings with a mean diameter 37.9 ± 1.2 nm (n = 8) that were observed without ligand (Figure 5B, insets). In comparison, IHB induced a 11.8 S main peak and single rings 24.9 ± 0.7 nm (n = 42) in diameter, whereas ERI reverted the 7.4 and 9.0 S oligomer peaks into 5.5 S tubulin dimers (Figure 5B) in agreement with previous results.[33] When GDP-tubulin was employed to enhance double ring formation, a $s^{10}_{20,w}$ = 36 S peak and abundant double rings with mean diameter 36.5 ± 0.3 nm (n = 153) were observed as expected.[25,36] Under these conditions PM050489 suppressed the double ring formation and induced $s^{10}_{20,w}$ = 15.6 S single rings with external diameter 25.8 ± 0.6 nm (n = 71), whereas IHB gave a 16.5 S hypersharp peak and 29.0 ± 0.5 nm (n = 73) diameter rings and ERI reduced the rings to oligomers (Figure 5C). The ring reshaping by PM050489 suggests that this ligand binds into the interdimer

dx.doi.org/10.1021/cb400461j | ACS Chem. Biol. 2013, 8, 2084−2094

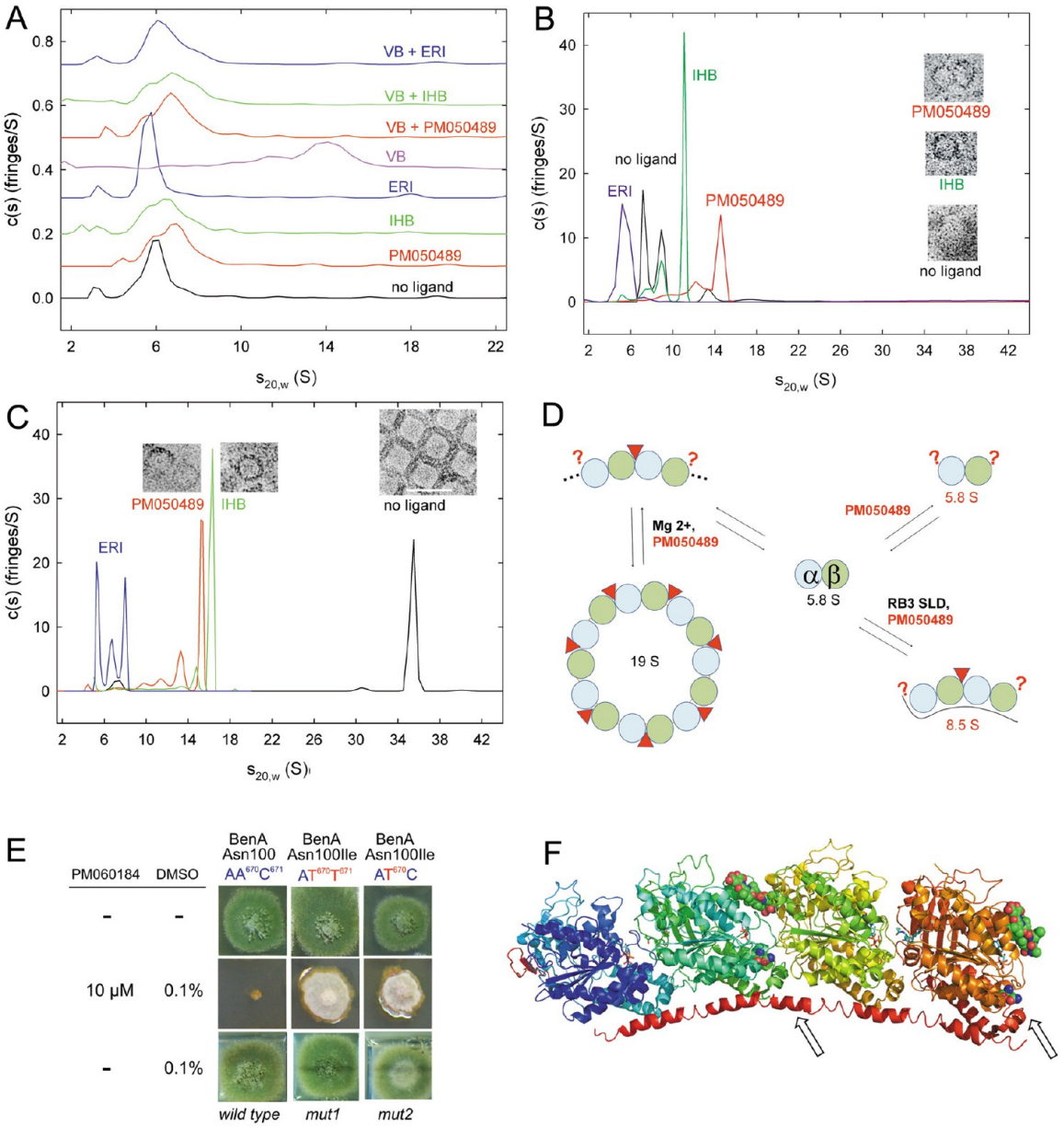

Figure 5. Effects of PM050489 and Vinca domain ligands on tubulin self-association. Binding site mapping. The sedimentation coefficient distributions $c(s)$ shown were obtained by analytical ultracentrifugation with interference optics under various representative conditions. (A) 5 μM tubulin in 1.1 mM free Mg^{2+} (black trace, 3 mM $MgCl_2$ and 0.1 mM GTP in PE buffer pH 7.0, at 37 °C). The effects of 5 μM PM050489 (red), isohomohalichondrin B (IHB, green), eribulin (ERI, blue), vinblastine (VBL, pink), and combinations of these are shown by the corresponding profiles. (B) 100 μM tubulin in 6.7 mM free Mg^{2+} with 1 mM GTP (black trace, 12 mM $MgCl_2$ in PE buffer pH 6.5, at 20 °C). Double-concentric rings were visualized by negative stain electron microscopy (inset). The effects of 100 μM PM050489, isohomohalichondrin B, and eribulin are shown by the correspondingly colored profiles. Under these conditions vinblastin induced the formation of tubulin precipitates sedimenting to the bottom of the cell during acceleration. (C) Same as panel B but with 1 mM GDP (6.8 mM free Mg^{2+}) to markedly enhance double ring formation (inset, the bar indicates 50 nm), which reshape into single rings with PM050489 and IHB (insets). (D) A model scheme of the proposed interfacial binding of PM050489 (red symbols) to tubulin dimers, oligomers, single rings, and T_2R complexes. The RB3 SLD is represented by the black curved line. The sedimentation coefficient value of the ligand-T_2R complex is uncorrected. (E) Growth of wild type *A. nidulans* and mutants carrying the mutations AAC to ATT or AAC to ATC, in BenA (β-tubulin) codon 100 (wild-type and mutant nucleotides in blue and red, respectively). Strains were cultured in the presence or absence of 10 μM PM060184 and 0.1% DMSO, as indicated. The two different base changes result in the same Asn100Ile aminoacid substitution in BenA. *A. nidulans* colonies are green due to the color of the asexual spores (conidia) that develop in reproductive structures (denoted conidiophores) on the surface of vegetative hyphae. Unlike the wild-type, Asn100Ile BenA mutants are able to form colonies on 10 μM PM060184, even though their conidiation is prevented, which results in colonies with a white surface. This might reflect the possibility that conidiation is more sensitive to PM060184 than vegetative growth. Residual 0.1% v/v DMSO does not affect conidiation. Note that the mutations in *benA* do not affect growth or prevent conidiation on medium without PM060184 (see text for discussion). (F) Scheme showing the position of β-tubulin Asn100 compared to the phomopsin A molecules bound to $\alpha\beta$-tubulin dimers in the T_2R complex (Protein Data Bank entry 3DU7, displayed with PyMOL in the same orientation as in panel D). The arrows point to Asn100, which is represented as the larger phomopsin A by color coded atom spheres. Both Asn100 and phomopsin are at the β-tubulin plus ends, at the free end (right) and at the interface between tubulin

dx.doi.org/10.1021/cb400461j | *ACS Chem. Biol.* 2013, 8, 2084−2094

Figure 5. continued

dimers (middle), but occupy different positions. Bound guanine nucleotides and colchicine are shown in sticks. Notice that Asn100 is located at the inside of the curved structure, opposite to the arbitrary drawing of the ligand at the outside in panel D.

interfaces of the small curved single rings, where it fits better than into the less curved larger rings. The external diameter of the PM050489 rings approximately corresponds to 7 tubulin dimers.[36] The sedimentation coefficient of these PM050489-induced single rings, once corrected for concentration,[25] is $s^0_{20,w}$ = 18.8 ± 0.6 S. Modeling the hydrodynamics of tubulin single rings made of 6, 7, or 8 dimers associated head to tail with WinHydro++[39] gave calculated $s^0_{20,w}$ values of 18.0, 18.9, and 19.7 S respectively, supporting that the PM050489-induced rings are made of 7 ± 1 tubulin dimers.

The above results further support the binding of PM050489 to the tubulin interdimer interface. This ligand modulates the Mg^{2+}-induced association of $\alpha\beta$-dimers, resulting in 19 S single ring formation, more similarly to IHB than to ERI, but completely different from VBL. PM050489 binding reshapes tubulin double rings into smaller rings with a different curvature. This suggests that the tubulin interdimer interface accommodates PM050489 with a propagated structural distortion. Several Vinca domain ligands are known to induce formation of tubulin single rings, including cryptophicin 52 [15−17 S, 9 tubulin dimers[40]], cryptophicin 1 [15 S, 8 tubulin dimers[41]], and dolastatin 10 [20 S, 14 tubulin dimers[41,42]]. The HIV-1 protein Rev induces bilayered rings made of 2×(14−16) tubulin dimers,[43] and kinesin pKinI induces single rings [13 tubulin dimers[44]], both of them binding to the inside of the rings, which highlights the flexibility of tubulin protofilaments.

Binding of PM050489 to the Tubulin-RB3 SLD Complex. Stathmin is a cellular microtubule inhibitor implicated in signal transduction and disease, which forms a complex with two $\alpha\beta$-tubulin dimers in curved conformation (T_2S).[45] Stathmin is a mediator of VBL activity,[46] and related ligands can enhance or inhibit the formation of the T_2S complex.[33] We examined whether PM050489 binding modulates the formation of the similar complex of tubulin (T) with the SLD of protein RB3 (T_2R), employing sedimentation velocity experiments in which the protein association and ligand co-sedimentation with T and T_2R are simultaneously measured.[47] Puzzlingly, we found that PM050489 only marginally enhances the T_2R complex formation and binds similarly to T and T_2R (Supplementary Figure S5). This indicates similar affinities for both tubulin association species. For comparison, we confirmed that VBL binds to T_2R complexes, strongly enhancing their formation (Supplementary Figure S6). The stoichiometry of PM050489 binding to the T_2R complex formed in an excess of RB3 SLD was 0.93 ± 0.02 ligand per tubulin dimer, compared to 0.94 ± 0.05 ligand per isolated tubulin dimer under the same conditions (determined by HPLC, Supplementary Figure S7). That the binding of PM050489 reshapes tubulin rings and permits the T_2R complex formation may be explained if upon binding of the ligand at one or both subunits at the interdimer interface there is a loss of protein−protein interactions upon deformation of the T_2R complex or if the ligand binding pose changes, compensating for the additional free energy change expected upon interfacial ligand binding with respect to binding to the tubulin dimer free end. Since PM050489 binding to microtubules was not detected, interfacial binding would take place only at one microtubule end rather than within the microtubule body.

Mapping the PM05489/PM060184 Binding Site. The biochemical and AUC results all together suggest that PM050489 binds to one end of the tubulin dimer, either at the plus end of the β-subunit or at the minus end of the α-subunit. Binding to the 19 S tubulin single rings induced by this ligand is also expected to take place at the interdimer interfaces. According to the binding stoichiometry, the ligand should also bind between tubulin dimers in the T_2R complex (see the scheme in Figure 5D, noticing that this ligand could equally bind to the inside instead of the ouside of the rings and T_2R complex). We examined the effect of pironetin, which inhibits VBL binding and covalently reacts with α-Lys 354,[48] at the minus end of α-tubulin, but the pironetin-tubulin adduct formation bound PM050489 similarly to unmodified tubulin. On the other hand, the N-terminal β-hairpin of RB3 also binds at the minus end of α-tubulin,[23] but this did not modify the ligand binding in the T_2R complex, suggesting PM050489 binding to the plus end of the β-subunit.

In order to map the binding site we used the filamentous fungus *Aspergillus nidulans*, a genetically amenable eukaryote in which α-, β-, and γ-tubulin genes were first identified (reviewed in refs 49 and 50). *A. nidulans* β-tubulin (BenA) is ∼80% identical to human β-tubulin (neural isotypes 2 and 3 and non-neural isotype 5). *A. nidulans* colony formation on solid growth medium is virtually abolished by 10 μM PM060184 (Supplementary Figure S8A). Fluorescence microscopy observations of hyphal cells expressing GFP-tagged α-tubulin before and after the addition of the drug revealed that PM060184 induces the rapid (<10 min) relocalization of α-tubulin-GFP from the microtubules to the cytoplasm (Supplementary Figure S8B), demonstrating that the drug destabilizes microtubules *in vivo*.

Sensitivity to PM060184 allowed us to select for mutants resistant to this compound (10 μM) after UV mutagenesis, in which we sequenced the *tubA* and *benA* genes coding for the major α- and β-tubulin isoforms, respectively. We identified two different missense mutations (AAC to ATC and AAC to ATT), both resulting in the substitution of the conserved asparagine 100 by isoleucine (Asn100Ile) in BenA (β-tubulin). Unlike the wild type, strains carrying these mutations grow well on 10 μM PM060184 (Figure 5E). For one of these mutants, we established that the resistance phenotype displays Mendelian segregation in genetic crosses, showing that the resistance phenotype results from a single mutational hit. Moreover, we further established that the resistance mutation is genetically linked to the chromosome VIII sulfate utilization mutation *sD85*. The genetic distance determined from 96 progeny from a heterozygous cross is 8.3 cM, which is not significantly different from that reported between *sD* and *benA* (5.6 cM, http://www.fgsc.net/Aspergillus/gene_list/; χ-square test P value = 0.2441). These results show beyond doubt that resistance to PM060184 is due to the mutant β-tubulin allele. Interestingly, Asn100Ile-BenA mutants grow like the wild type in the absence of PM060184 (Figure 5E), indicating that the mutation does not significantly affect microtubule-dependent functions *in vivo*. This suggests that resistance in Asn100Ile-BenA mutants is achieved by direct modification of the PM060184 binding site in β-tubulin, preventing the drug effect

by inhibiting its binding rather than by altering microtubule assembly dynamics. Therefore, Asn100 on β-tubulin critically contributes to the binding of PM060184 *in vivo*. Of note, β-tubulin Asn100Ile mutants have been previously selected in *A. nidulans* as conferring resistance to the antimicrotubule drug Rhizoxin.[51] The Asn100 residue is in fact located at the plus end of β-tubulin, which can be free or contacting another tubulin dimer. However, Asn100 is in a clearly different position from VBL and the Vinca domain, exemplified by phomposin A (Figure 5F). Our genetic results thus suggest that the antitumor compound PM060184 binds to a new locus in β-tubulin that is defined by the position of Asn100.

Interfacial binding of the Vinca domain ligands induces tubulin protofilament curvature, which underlies the inhibition of microtubule assembly dynamics and their antitumor activities. The unique properties of PM050489 consist of its much higher affinity for tubulin dimers than Vinca domain ligands, but with effects on tubulin self-association different from those of VBL. We thus suggest that high affinity binding of PM050489 and its analogues at the microtubule plus end is the cause of its powerful microtubule inhibitory and antiproliferative activities. These features are of interest for structural studies and the development of this new chemotype into an effective antitumor drug.

Conclusions. The results of this work indicate that the new antiproliferative marine-derived compound PM050489 and its analogue PM060184 bind to tubulin dimers at the β-tubulin plus end with the highest known affinities among tubulin-binding agents. These small molecules target the longitudinal association between tubulin dimers, possibly at a new site rather than at the vinblastine site according to resistance mutations, and thus inhibit microtubule assembly. More similarly to isohomohalichondrin B than to its analogue eribulin and distinctly from vinblastine, their binding only weakly induces association of $\alpha\beta$-tubulin dimers. Possibly acting like a hinge, PM050489 reshapes Mg^{2+}-induced tubulin double rings into smaller 19 S single rings made of 7 $\pm$ 1 $\alpha\beta$-tubulin dimers. PM050489 also binds to the complex of two head-to-tail tubulin dimers with the RB3 stathmin-like domain, with similar affinity as to isolated tubulin dimers. The hydroxyl analogue PM060327 binds to tubulin in an extended conformation, as indicated by TR-NOESY NMR. These new inhibitors disrupt cellular microtubules at subnanomolar concentrations, probably by binding to their plus end, and thus block mitosis. They inhibit the proliferation of 10 different types of cultured human tumors more effectively than vinblastine or paclitaxel. A parallel study, to be reported elsewhere, has shown that they are potent inhibitors of microtubule plus end dynamics in cells and effective against multidrug-resistant tumors *in vivo*. Our results reveal the target and the biochemical mechanism of action of these cytotoxic small molecules and encourage structural studies of their tubulin complexes and evaluation as potential antitumor drugs to be added to the currently employed tubulin binding agents. PM060184 is undergoing phase I clinical trials in patients with advanced tumors.

METHODS

Small Molecules. PM050489, PM060184, and PM060327 were obtained by total synthesis at PharmaMar,[16] where PM060327 is an intermediate in the synthesis of PM050489. They were >95% pure when analyzed in an Agilent 1100 series HPLC, employing a ZORBAX Eclipse XDB-C18 column and a methanol/water gradient from 60% to 90% at 1 mL/min in 30 min. Cryptophyicin 1, auristatin, and dolastatin 10 were from the NIH compound repository. Eribulin was kindly provided by E. Hamel from the National Cancer Institute (Bethesda, MD). Isohomohalichondrin B was from PharmaMar.[52] Paclitaxel was provided by the late M. Suffness from the National Cancer Institute (Bethesda, MD). The colchicine analogue MTC was provided by Dr. T. J. Fizgerald, Florida A&M University. Docetaxel was provided by Rhône Poulenc Rorer, Aventis (Schiltigheim, France). Vinblastin was from Sigma Aldrich, and ^{3}H-vinblastin (555 GBq/mmol) was from GE Healthcare. Compounds were dissolved in d_6-DMSO to a final concentration of 10 mM and stored at −80 °C. Residual d_6-DMSO was <0.5% in cellular experiments and 1% in biochemical experiments unless noted.

Human Cell Methods. Human A549 non-small lung carcinoma cells were cultured as previously described.[53] The cell growth inhibition experiments were performed using the MTT assay in three independent experiments performed in triplicate as reported.[54,55] Flow cytometric cell cycle analyses and indirect immunofluorescence were performed as previously described after treatment of cells with the compounds at different concentrations for 20 h.[56]

Tubulin Biochemistry and Ligands Binding. Calf brain tubulin was purified[57] and prepared in homogeneous GDP and GTP bound forms as described.[58] Glutaradehyde-stabilized microtubules with active paclitaxel binding sites were prepared as described.[59,60] Critical tubulin concentrations of tubulin in the presence of ligands were measured as described.[56] The polymers formed were adsorbed onto Formvar/carbon-coated copper grids, stained with 1% uranyl acetate, and observed with a JEOL 1230 electron microscope operated at 100 kV and equipped with a Gatan Bioscan 702 CCD camera.

Ligands binding to stabilized microtubules was analyzed by sedimentation and HPLC. PM050489 or PM060184 (5 μM) were incubated for 30 min at 37 °C with an excess of paclitaxel binding sites (up to 70 μM) in stabilized microtubules, in 10 mM sodium phosphate, 3.4 M glycerol, 1 mM EGTA, 6 mM Cl_2Mg, 0.1 mM GTP, pH 6.5 (GAB). Samples were centrifuged for 20 min at 50,000 rpm in a TLA 100 rotor at 37 °C in a Beckman Optima TLX ultracentrifuge. The supernatants were collected, and the pellets were resuspended in 10 mM sodium phosphate pH 7.0. Supernatants and pellets were extracted three times with 1 volume of dichloromethane, dried, resuspended in 35 μL 60% methanol/water, and analyzed by HPLC as above. The compounds were detected and quantified by absorbance at 234 nm. To analyze ligands binding to native microtubules, 20 μM PM050489 or PM060184 was incubated with 50 μM assembling tubulin in GAB for 30 min at 37 °C. The microtubules formed were collected by centrifugation, and the samples were analyzed as described above.

Ligands binding to dimeric tubulin was measured by high-speed centrifugation. Samples (1 mL) containing 5 μM tubulin and 4 μM PM050489, PM060184, or PM060327, in the presence or absence of 50 μM nocodazol, auristatin, dolastatin 10, or cryptophicin 1, were incubated for 30 min at 37 °C in 10 mM sodium phosphate, 1.5 mM $MgCl_2$, 1 mM EDTA, 0.1 mM GTP pH 7.0 buffer (PE 1.5) in polycarbonate centrifuge tubes (Beckman). The samples were then centrifuged at 100,000 rpm for 1 h at 37 °C in a TLA120 rotor in the Beckman Optima TLX ultracentrifuge. The upper and lower 500 μL of the solution were carefully collected, and any pellets were resuspended in 10 mM phosphate buffer pH 7.0. The upper fraction is depleted of protein and contains free ligand. Controls in the absence of tubulin confirmed that the ligand remained soluble during the experiment. The tubulin concentrations in the three fractions were measured by the Bradford assay (BioRad), and 10 μM docetaxel was added as internal standard. The samples were extracted and analyzed by HPLC as described above.

The effect of PM050489 on vinblastin binding was measured using ^{3}H-vinblastine. Samples of 500 nM tubulin in PE 1.5 with 500 nM ^{3}H-vinblastine in the presence of up to 5 μM PM050489 or up to 50 μM dolastatin 10 were incubated for 30 min at 37 °C and centrifuged as above. The upper and lower 500 μL of the solution were carefully collected, and 300 μL of each sample was mixed with 1.2 mL of ReadySafe solution (Beckman). The concentration of free and bound ^{3}H-vinblastine was determined by scintillation counting in an Rackbeta

1219 (LKB Wallac) after correction by the sedimentation factor determined as described.[61] The effect of PM050489 on the binding of the colchicine analogue MTC (2-methoxy-5-(2,3,4-trimethoxyphenyl)-2,4,6-cycloheptatrien-1-one), which becomes fluorescent in complex with tubulin, was determined as described.[21]

To measure the affinity of PM060327 binding to tubulin, 3.5-mL samples containing 20 nM PM060327 and 0−400 nM tubulin in PE 1.5 buffer were incubated as above and centrifuged at 100,000 rpm for 2 h at 37 °C in a TLA100.4 rotor, and the upper half and lower half of the solution and pellet were separated. Then 30 nM docetaxel internal standard was added, and the samples were lyophilized, extracted three times with 1 mL of methanol, dried, redissolved in 50 μL of 60% methanol/water, and analyzed by HPLC as above. At this low ligand concentration, only 10 nM PM060327 remained available for interaction with a tubulin excesss (10−40 μM) in the polycarbonate ultracentrifuge tubes. The tubulin concentrations were also corrected for a 50% loss from the bottom fraction, due to pelleting or adsorption to the tube. This factor was determined spectrofluorometrically, employing spectrophotomerically calibrated tubulin standards on parallel 200−1,000 nM tubulin samples.

Sedimentation Velocity, Ligand Binding Stoichiometry, and Hydrodynamic Models. AUC experiments were done at 45,000 rpm and 20, 25, or 37 °C with a Beckman Optima XL-I analytical ultracentrifuge equipped with interference and absorbance optics, using an eight-hole An50Ti rotor and 1.2 cm Epon double-sector centerpieces. Apparent sedimentation coefficients were determined by the sedimentation coefficient distribution $c(s)$ generated with SEDFIT[62] and were corrected to water at 20 °C using the solutions density and viscosity and SEDNTERP.[63] The interference optics was employed to measure tubulin sedimentation and radial absorbance data at 310 nm were acquired to measure the PM050489 ligand. The area under the peak in the $c(s)$ distribution of the ligand and initial scans at 3,000 rpm were employed to calculate the fraction of ligand co-sedimenting with the protein.[47]

The sedimentation coefficient of tubulin single rings was corrected by concentration employing the previously determined correction for the concentration dependence of the sedimentation coefficient of tubulin double rings and dimers, which are similar ($s^C = s^0(1 - gC)$, where C is the tubulin concentration (g/L) and g = 0.019 L/g[25]). The corrected sedimentation coefficient of double rings was $s^0_{20,w}$ = 44 S, in agreement with the known value of 42 ± 2 S.[25] The theoretical sedimentation coefficients of tubulin ring models were calculated with WinHydro++1.0.[39] Models were constructed with a variable pair number (..., 12, 14, 16, ...) of 4.25-nm-spaced tubulin monomers.[36] Each monomer was simulated by an equivalent sphere of 3.36 nm radius, since a model tubulin dimer with two of these spheres fitted the experimental sedimentation coefficient value of 5.8 S. The sedimentation coefficient of similarly constructed double rings made of 12 + 16 tubulin dimers[36] with a mean diameter of 38 nm, calculated as a control, was 41 S.

NMR Methods. The samples of dimeric tubulin with ligands were prepared as described[30] in 10 mM sodium phosphate buffer, 0.1 mM GTP made in D_2O, apparent pH 7.0. To bring the solubility of PM060327 into a practical range for NMR measurements, it was necessary to increase the d_6-DMSO concentration in the buffer to 7.5%. NMR spectra were recorded at 310 K with Bruker 600 MHz spectrometer equipped with a cryoprobe as described.[30] STD experiments were acquired with 1,000 scans and a saturation time of 2 s. TR-NOESY were measured with 152 scans and a mixing time of 200 ms.

***A. nidulans* Strains, Media, Genetic Methods, and Microscopy.** Growth media and genetic methodologies were as previously described.[64] All strains carried markers in standard use.

Mutagenesis was performed by ultraviolet irradiation of *A. nidulans* (strain MAD2: *biA1*) asexual conidiospores for 17 min using Stratagene's Stratalinker UV cross-linker (surface power density = 0.02 mW/cm^2), which resulted in 97.5% lethality. Spores (10^8) were plated on standard complete medium Petri dishes (150 cm^2 surface), supplemented with biotin as appropriate, 10 μM PM060184, and 1% DMSO, and were incubated for 4 days at 37 °C. Following this process strains MAD4649 [biA1; (AAC669,670,671ATC)-*benA*] and MAD4654 [biA1; (AAC669,670,671ATT)-*benA*] were obtained. For outcrosses of the mutant strains, MAD3688 (*wA3; pantoB100*) and MAD4655 (*choC3 fwA1 sD85*) were used.

For sequencing of *A. nidulans tubA* and *benA* genes the following DNA primers were used: *tubAfw* (5-cttctcgttctccaatttcaccc-3), *tubArev* (5-gccagcgtatcacctagactacc-3), *tubAfw2* (5-gcgtctctctgtcgactacggc-3), *tubArev2* (5-ccatgaagctgcagtcggag-3) *benAfw* (5-ccagtctatcttcatccgac-ttcg-3), *benArev* (5-ccaggggtattattatgagctgatc-3), benAfw2 (5-gccaccctt-tccgttcacc-3), *benArev3* (5-gggtgcgcatgcagatatcg-3).

In vivo fluorescence microscopy was performed as previously described[64] using strain MAD2023 (pyrG89; sc12; choA1; chaA1 tubA::gfp, provided by B. R. Oakley).

■ ASSOCIATED CONTENT

Ⓢ Supporting Information

Supplementary table and figures. This material is available free of charge via the Internet at http://pubs.acs.org.

■ AUTHOR INFORMATION

Corresponding Author

*E-mail: fer@cib.csic.es; j.m.andreu@cib.csic.es.

Present Address

[§]Memorial Sloan-Kettering Cancer Center, Rockefeller Research Laboratories, 430 East 67th Street, New York, NY 10065, USA.

Notes

The authors declare the following competing financial interest(s): L.F.G.-F., V.M, C.M.G., and C.C. are employees and shareholders of PharmaMar, which has commercial interest in the compounds described.

■ ACKNOWLEDGMENTS

We wish to thank J. M. Fernandez Sousa (PharmaMar) for useful discussions and support, E. Hamel (NCI) for providing eribulin, C. Scazzocchio and G. Diallinas for useful advice on mutant screening, H. N. Arst for advice on mutant screening and mapping and for kindly providing strains MAD3688 and MAD4655, T. J. Fitzgerald (A&M University) for MTC and C. Alfonso (CIB) for AUC analysis. We also thank Rhône Poulenc Rorer Aventis for supplying docetaxel and Matadero Municipal Vicente de Lucas de Segovia for providing the calf brains for tubulin purification. B.P. had a contract from Comunidad de Madrid, and A.C. had a Ramon y Cajal contract, J.R.-S. had a fellowship from "Programa de Cooperación Científica entre el Ministerio de Ciencia, Tecnologías y Medio Ambiente de la República de Cuba (CITMA) y el CSIC". This work was supported by grants BIO2010-16351 (J.F.D.), BQU2009-08536 (J.J.-B.), CAM S2010/BMD-2457 (J.F.D.), CAM S2010/BMD-2353 (J.J.-B., J.M.A.), IPT-2011-0752-900000 and BIO2012-30965 (M.A.P.), BFU2011-23416 (J.M.A.) and PharmaMar-CSIC contracts.

■ DEDICATION

J.M.A. and J.F.D. wish to dedicate this paper to S. N. Timasheff for his inspiring work on tubulin-vinblastine interactions.[26,27]

■ REFERENCES

(1) Jordan, M. A., Wendell, K., Gardiner, S., Derry, W. B., Copp, H., and Wilson, L. (1996) Mitotic block induced in HeLa cells by low concentrations of paclitaxel (Taxol) results in abnormal mitotic exit and apoptotic cell death. *Cancer Res. 56*, 816−825.

(2) Jordan, M. A., and Kamath, K. (2007) How do microtubule-targeted drugs work? An overview. *Curr. Cancer Drug Targets 7*, 730–742.
(3) Johnson, I. S., Wright, H. F., Svoboda, G. H., and Vlantis, J. (1960) Antitumor principles derived from Vinca rosea Linn. I. Vincaleukoblastine and leurosine. *Cancer Res. 20*, 1016–1022.
(4) Schiff, P. B., Fant, J., and Horwitz, S. B. (1979) Promotion of microtubule assembly in vitro by taxol. *Nature 277*, 665–667.
(5) Gueritte-Voegelein, F., Guenard, D., Lavelle, F., Le Goff, M. T., Mangatal, L., and Potier, P. (1991) Relationships between the structure of taxol analogues and their antimitotic activity. *J. Med. Chem. 34*, 992–998.
(6) Jordan, M. A., and Wilson, L. (2004) Microtubules as a target for anticancer drugs. *Nat. Rev. Cancer 4*, 253–265.
(7) Galsky, M. D., Dritselis, A., Kirkpatrick, P., and Oh, W. K. (2010) Cabazitaxel. *Nat. Rev. Drug Discovery 9*, 677–678.
(8) Dumontet, C., Jordan, M. A., and Lee, F. F. (2009) Ixabepilone: targeting betaIII-tubulin expression in taxane-resistant malignancies. *Mol. Cancer Ther. 8*, 17–25.
(9) Pean, E., Klaar, S., Berglund, E. G., Salmonson, T., Borregaard, J., Hofland, K. F., Ersboll, J., Abadie, E., Giuliani, R., and Pignatti, F. (2012) The European medicines agency review of eribulin for the treatment of patients with locally advanced or metastatic breast cancer: summary of the scientific assessment of the committee for medicinal products for human use. *Clin. Cancer Res. 18*, 4491–4497.
(10) Kaiser, J. (2011) Combining targeted drugs to stop resistant tumors. *Science 331*, 1542–1545.
(11) Eckford, P. D. W., and Sharom, F. J. (2009) ABC efflux pump-based resistance to chemotherapy drugs. *Chem. Rev. 109*, 2989–3011.
(12) Goldman, B. (2003) Multidrug resistance: can new drugs help chemotherapy score against cancer? *J. Natl. Cancer Inst. 95*, 255–257.
(13) Burkhard, L. P., Cook, P. M., and Mount, D. R. (2003) The relationship of bioaccumulative chemicals in water and sediment to residues in fish: a visualization approach. *Environ. Toxicol. Chem. 22*, 2822–2830.
(14) Paterson, I., and Anderson, E. A. (2005) Chemistry. The renaissance of natural products as drug candidates. *Science 310*, 451–453.
(15) Miller, J. H., Singh, A. J., and Northcote, P. T. (2010) Microtubule-stabilizing drugs from marine sponges: Focus on peloruside A and zampanolide. *Mar. Drugs 8*, 1059–1079.
(16) Martin, M. J., Coello, L., Fernandez, R., Reyes, F., Rodriguez, A., Murcia, C., Garranzo, L., Mateo, C., Sanchez, F., Bueno, S., de Eguilior, C., Francesch, A. M., Munt, S., and Cuevas, C. (2013) Isolation and first total synthesis of PM050489 and PM060184, two new marine anticancer compounds. *J. Am.Chem. Soc. 135*, 10164–10171.
(17) Jordan, M. A., Thrower, D., and Wilson, L. (1992) Effects of vinblastine, podophyllotoxin and nocodazole on mitotic spindles - implications for the role of microtubule dynamics in mitosis. *J. Cell Sci. 102*, 401–416.
(18) Hamel, E., and Covell, D. G. (2002) Antimitotic peptides and depsipeptides. *Curr. Med. Chem. Anticancer Agents 2*, 19–53.
(19) Huyck, T. K., Gradishar, W., Manuguid, F., and Kirkpatrick, P. (2011) Eribulin mesylate. *Nat. Rev. Drug Discovery 10*, 173–174.
(20) Menendez, M., Rivas, G., Diaz, J. F., and Andreu, J. M. (1998) Control of the structural stability of the tubulin dimer by one high affinity bound magnesium ion at nucleotide N-site. *J. Biol. Chem. 273*, 167–176.
(21) Andreu, J. M., Gorbunoff, M. J., Lee, J. C., and Timasheff, S. N. (1984) Interaction of tubulin with bifunctional colchicine analogues: an equilibrium study. *Biochemistry 23*, 1742–1752.
(22) Ravelli, R. B., Gigant, B., Curmi, P. A., Jourdain, I., Lachkar, S., Sobel, A., and Knossow, M. (2004) Insight into tubulin regulation from a complex with colchicine and a stathmin-like domain. *Nature 428*, 198–202.
(23) Gigant, B., Wang, C., Ravelli, R. B., Roussi, F., Steinmetz, M. O., Curmi, P. A., Sobel, A., and Knossow, M. (2005) Structural basis for the regulation of tubulin by vinblastine. *Nature 435*, 519–522.
(24) Pommier, Y., and Marchand, C. (2012) Interfacial inhibitors: targeting macromolecular complexes. *Nat. Rev. Drug Discovery 11*, 250–250.
(25) Frigon, R. P., and Timasheff, S. N. (1975) Magnesium-induced self-association of calf brain tubulin. I. Stoichiometry. *Biochemistry 14*, 4559–4566.
(26) Na, G. C., and Timasheff, S. N. (1986) Interaction of vinblastine with calf brain tubulin–effects of magnesium ions. *Biochemistry 25*, 6222–6228.
(27) Na, G. C., and Timasheff, S. N. (1980) Thermodynamic linkage between tubulin self-association and the binding of vinblastine. *Biochemistry 19*, 1355–1365.
(28) Smith, J. A., Wilson, L., Azarenko, O., Zhu, X., Lewis, B. M., Littlefield, B. A., and Jordan, M. A. (2010) Eribulin binds at microtubule ends to a single site on tubulin to suppress dynamic instability. *Biochemistry 49*, 1331–1337.
(29) Bai, R., Tam Luong, N., Burnett, J. C., Atasoylu, O., Munro, M. H. G., Pettit, G. R., Smith, A. B., III., Gussio, R., and Hamel, E. (2011) Interactions of halichondrin B and eribulin with tubulin. *J. Chem. Inf. Model. 51*, 1393–1404.
(30) Canales, A., Salarichs, J. R., Trigili, C., Nieto, L., Coderch, C., Andreu, J. M., Paterson, I., Jiménez-Barbero, J., and Díaz, J. F. (2011) Insights into the interaction of discodermolide and docetaxel with dimeric tubulin. Mapping the binding sites of microtubule-stabilizing agents using an integrated NMR and computational approach. *ACS Chem. Biol. 6*, 789–799.
(31) Lobert, S., Ingram, J. W., and Correia, J. J. (2007) The thermodynamics of vinca alkaloid-induced tubulin spirals formation. *Biophys. Chem. 126*, 50–58.
(32) Dabydeen, D. A., Burnett, J. C., Bai, R., Verdier-Pinard, P., Hickford, S. J., Pettit, G. R., Blunt, J. W., Munro, M. H., Gussio, R., and Hamel, E. (2006) Comparison of the activities of the truncated halichondrin B analog NSC 707389 (E7389) with those of the parent compound and a proposed binding site on tubulin. *Mol. Pharmacol. 70*, 1866–1875.
(33) Alday, P. H., and Correia, J. J. (2009) Macromolecular interaction of halichondrin B analogues eribulin (E7389) and ER-076349 with tubulin by analytical ultracentrifugation. *Biochemistry 48*, 7927–7938.
(34) Kirschner, M. W., Williams, R. C., Weingarten, M., and Gerhart, J. C. (1974) Microtubules from mammalian brain: Some properties of their depolymerization products and a proposed mechanism of assembly and disassembly. *Proc. Natl. Acad. Sci. U.S.A. 71*, 1159–1163.
(35) Melki, R., Carlier, M. F., Pantaloni, D., and Timasheff, S. N. (1989) Cold depolymerization of microtubules to double rings: geometric stabilization of assemblies. *Biochemistry 28*, 9143–9152.
(36) Díaz, J. F., Pantos, E., Bordas, J., and Andreu, J. M. (1994) Solution structure of GDP-tubulin double rings to 3 nm resolution and comparison with microtubules. *J. Mol. Biol. 238*, 214–225.
(37) Elie-Caille, C., Severin, F., Helenius, J., Howard, J., Muller, D. J., and Hyman, A. A. (2007) Straight GDP-tubulin protofilaments form in the presence of taxol. *Curr. Biol. 17*, 1765–1770.
(38) Wang, H. W., and Nogales, E. (2005) Nucleotide-dependent bending flexibility of tubulin regulates microtubule assembly. *Nature 435*, 911–915.
(39) García de la Torre, J., del Rio Echenique, G., and Ortega, A. (2007) Improved calculation of rotational diffusion and intrinsic viscosity of bead models for macromolecules and nanoparticles. *J. Phys. Chem. B 111*, 955–961.
(40) Barbier, P., Gregoire, C., Devred, F., Sarrazin, M., and Peyrot, V. (2001) In vitro effect of cryptophycin 52 on microtubule assembly and tubulin: molecular modeling of the mechanism of action of a new antimitotic drug. *Biochemistry 40*, 13510–13519.
(41) Watts, N. R., Cheng, N. Q., West, W., Steven, A. C., and Sackett, D. L. (2002) The cryptophycin-tubulin ring structure indicates two points of curvature in the tubulin dimer. *Biochemistry 41*, 12662–12669.

(42) Moores, C. A., and Milligan, R. A. (2008) Visualisation of a kinesin-13 motor on microtubule end mimics. *J. Mol. Biol. 377*, 647–654.
(43) Watts, N. R., Sackett, D. L., Ward, R. D., Miller, M. W., Wingfield, P. T., Stahl, S. S., and Steven, A. C. (2000) HIV-1 Rev depolymerizes microtubules to form stable bilayered rings. *J. Cell Biol. 150*, 349–360.
(44) Moores, C. A., Yu, M., Guo, J., Beraud, C., Sakowicz, R., and Milligan, R. A. (2002) A mechanism for microtubule depolymerization by KinI kinesins. *Mol. Cell 9*, 903–909.
(45) Steinmetz, M. O. (2007) Structure and thermodynamics of the tubulin-stathmin interaction. *J. Struct. Biol. 158*, 137–147.
(46) Devred, F., Tsvetkov, P. O., Barbier, P., Allegro, D., Horwitz, S. B., Makarov, A. A., and Peyrot, V. (2008) Stathmin/Op18 is a novel mediator of vinblastine activity. *FEBS Lett. 582*, 2484–2488.
(47) Barbier, P., Dorleans, A., Devred, F., Sanz, L., Allegro, D., Alfonso, C., Knossow, M., Peyrot, V., and Andreu, J. M. (2010) Stathmin and interfacial microtubule inhibitors recognize a naturally curved conformation of tubulin dimers. *J. Biol. Chem. 285*, 31672–31681.
(48) Usui, T., Watanabe, H., Nakayama, H., Tada, Y., Kanoh, N., Kondoh, M., Asao, T., Takio, K., Nishikawa, K., Kitahara, T., and Osada, H. (2004) The anticancer natural product pironetin selectively targets Lys352 of alpha-tubulin. *Chem. Biol. 11*, 799–806.
(49) Oakley, B. R. (2004) Tubulins in Aspergillus nidulans. *Fungal Genet. Biol. 41*, 420–427.
(50) Morris, N. R., Efimov, V. P., and Xiang, X. (1998) Nuclear migration, nucleokinesis and lissencephaly. *Trends Cell Biol. 8*, 467–470.
(51) Takahashi, M., Matsumoto, S., Iwasaki, S., and Yahara, I. (1990) Molecular basis for determining the sensitivity of eucaryotes to the antimitotic drug rhizoxin. *Mol. Gen. Genet. 222*, 169–175.
(52) Garcia-Rocha, M., Garcia-Gravalos, M. D., and Avila, J. (1996) Characterisation of antimitotic products from marine organisms that disorganise the microtubule network: ecteinascidin 743, isohomohalichondrin-B and LL-15. *Br. J. Cancer 73*, 875–883.
(53) Buey, R. M., Calvo, E., Barasoain, I., Pineda, O., Edler, M. C., Matesanz, R., Cerezo, G., Vanderwal, C. D., Day, B. W., Sorensen, E. J., Lopez, J. A., Andreu, J. M., Hamel, E., and Díaz, J. F. (2007) Cyclostreptin binds covalently to microtubule pores and lumenal taxoid binding sites. *Nat. Chem. Biol. 3*, 117–125.
(54) Leal, J. F., Martinez-Diez, M., Garcia-Hernandez, V., Moneo, V., Domingo, A., Bueren-Calabuig, J. A., Negri, A., Gago, F., Guillen-Navarro, M. J., Aviles, P., Cuevas, C., Garcia-Fernandez, L. F., and Galmarini, C. M. (2010) PM01183, a new DNA minor groove covalent binder with potent in vitro and in vivo anti-tumour activity. *Br. J. Pharmacol. 161*, 1099–1110.
(55) Leal, J. F., Garcia-Hernandez, V., Moneo, V., Domingo, A., Bueren-Calabuig, J. A., Negri, A., Gago, F., Guillen-Navarro, M. J., Aviles, P., Cuevas, C., Garcia-Fernandez, L. F., and Galmarini, C. M. (2009) Molecular pharmacology and antitumor activity of Zalypsis in several human cancer cell lines. *Biochem. Pharmacol. 78*, 162–170.
(56) Buey, R. M., Barasoain, I., Jackson, E., Meyer, A., Giannakakou, P., Paterson, I., Mooberry, S., Andreu, J. M., and Díaz, J. F. (2005) Microtubule interactions with chemically diverse stabilizing agents: Thermodynamics of binding to the paclitaxel site predicts cytotoxicity. *Chem. Biol. 12*, 1269–1279.
(57) Andreu, J. M. (2007) Large scale tubulin purification with the modified Weisenberg procedure, In *Methods Mol. Med.* (Zhou, J., Ed.), pp 17–28, Humana Press Inc., Totowa, NJ.
(58) Díaz, J. F., and Andreu, J. M. (1993) Assembly of purified GDP-tubulin into microtubules induced by taxol and taxotere: reversibility, ligand stoichiometry, and competition. *Biochemistry 32*, 2747–2755.
(59) Díaz, J. F., Barasoain, I., and Andreu, J. M. (2003) Fast kinetics of Taxol binding to microtubules. Effects of solution variables and microtubule-associated proteins. *J. Biol. Chem. 278*, 8407–8419.
(60) Buey, R. M., Diaz, J. F., Andreu, J. M., O'Brate, A., Giannakakou, P., Nicolaou, K. C., Sasmal, P. K., Ritzen, A., and Namoto, K. (2004) Interaction of epothilone analogs with the paclitaxel binding site; relationship between binding affinity, microtubule stabilization, and cytotoxicity. *Chem. Biol. 11*, 225–236.
(61) Schaffner-Barbero, C., Gil-Redondo, R., Ruiz-Avila, L. B., Huecas, S., Lappchen, T., den Blaauwen, T., Diaz, J. F., Morreale, A., and Andreu, J. M. (2010) Insights into nucleotide recognition by cell division protein FtsZ from a mant-GTP competition assay and molecular dynamics. *Biochemistry 49*, 10458–10472.
(62) Schuck, P., Perugini, M. A., Gonzales, N. R., Howlett, G. J., and Schubert, D. (2002) Size-distribution analysis of proteins by analytical ultracentrifugation: strategies and application to model systems. *Biophys. J. 82*, 1096–1111.
(63) Laue, T. M., Shah, B. D., Ridgeway, T. M., Pelletier,S. L. (1992) Computer-aided interpretation of analytical sedimentation data for proteins., In *Analytical Ultracentrifugation in Biochemistry and Polymer Science* (Harding, S. E., Rowe,A. J. and Horton, J. C., Ed.), pp 90–125, Royal Society of Chemistry, Cambridge.
(64) Pinar, M., Pantazopoulou, A., and Peñalva, M. A. (2013) Live-cell imaging of *Aspergillus nidulans* autophagy: RAB1 dependence, Golgi independence and ER involvement. *Autophagy 9*, 1–20.